International Journal of Microwave and Wireless Technologies, 2017, 9(3), 481–491.
doi:10.1017/S1759078715001750

RESEARCH PAPER

Studying the nonlinear performance of an amplifying reflectarray antenna

IMAN ARYANIAN, ABDOLALI ABDIPOUR AND GHOLAMREZA MORADI

In this paper, significance of studying the nonlinear performance of amplifying reflectarray antenna is clarified by showing nonlinear behavior of the unit cell. Furthermore, the procedure for nonlinear analysis of amplifying reflectarray antenna is described and nonlinear analysis is verified by ADS software simulation. Moreover, a typical amplifying reflectarray antenna is designed considering the nonlinear behavior. Nonlinear analysis of the active aperture-coupled patch unit cell is performed using harmonic balance method considering nonlinear model of the amplifier. Then, the effect of nonlinear element in radiation pattern of the antenna is studied. Passive unit cell is simulated using full-wave analysis method considering infinite array approach, and scattering parameters of the unit cell is obtained. Next, these scattering parameters are transformed to admittance parameters and used in obtaining nonlinear response and harmonic distortion of the unit cell containing amplifier. Obtained results show up to 3.4 dB error in predicting pattern of the antenna with linear modeling of the active element.

Keywords: Active array antennas and components, Antenna design, Modeling and measurements

Received 21 July 2015; Revised 29 November 2015; Accepted 9 December 2015; first published online 8 January 2016

I. INTRODUCTION

A microstrip reflectarray antenna is a low-profile planar reflector that consists of microstrip patch arrays printed on a dielectric substrate which its surface is illuminated by a feed antenna. Each element of the array is designed to produce required reflection phase shift to form desired pattern. Phase shift in each cell can be obtained by different methods like varying the size of the resonating patches [1] or by a transmission line of proper length connected [2, 3] or aperture-coupled to the patches [4, 5]. Moreover, the phase can be controlled by active element in the structure of the antenna which gives the ability of controlling the pattern to have a reconfigurable antenna [6, 7]. Different methods are used to add reconfigurability to reflectarray antenna, using microstrip elements with an integrated electronic control, like micro-electro-mechanical systems (MEMs)-based structures [8], varactor-loaded patches [9–12], PIN diodes [13], or liquid crystal-based structures [14]. Furthermore, amplifying reflectarray antenna is a candidate to increase gain of the antenna in which, an amplifier is used in each unit cell of the antenna. This kind of antenna has been used in [15–17] to reach to power amplification from the antenna surface.

Power level on the surface of the antenna can be such that it necessitates nonlinear analysis of active reflectarray antenna when using amplifier or diodes in the unit cell of the antenna. In this paper, it is shown that power distribution on the antenna surface may cause some active elements of the antenna to behave nonlinear. In these cases, unit cell of active reflectarray antenna should be analyzed in a two-step process to consider nonlinear behavior of active element. First, passive radiation part should be simulated by a full-wave analysis method to obtain parameters of the passive part. For this purpose, unit cell of the antenna is simulated assuming infinite array and the active element is replaced by a two port network. Also, two spatial ports are considered for each polarization of the incident plane wave which are modeled as Floqute port. Consequently, linear structure is analyzed to obtain scattering parameters of the unit cell. Next, obtained scattering parameters are used in the nonlinear analysis of the unit cell and finally nonlinear results are used in the design of whole antenna. The novelty of this paper is showing the importance of nonlinear analysis of amplifying reflectarray antenna which is not considered in the past works and also showing the effects of nonlinear phenomena on the antenna pattern. Furthermore, nonlinear analysis of amplifying reflectarray antenna is explained for the first time and the results are compared with simulation using ADS software. In addition, based on the described approach in this paper, one can develop the nonlinear analysis for the active reflectarray antenna with different nonlinear active devices by other nonlinear models. However, the described analysis method can be performed when nonlinear model of the active element is available. Nonlinear model may be provided by the constructor of the transistor or can be obtained from a test procedure to extract parameters of the nonlinear model which is performed for example in [18].

II. UNIT CELL CONFIGURATION

The proposed unit cell consists of a dual-polarized aperture-coupled microstrip patch and an amplifier connected

Department of Electrical Engineering, Amirkabir University of Technology, Tehran 15914, Iran
Corresponding author:
G. Moradi
Email: ghmoradi@aut.ac.ir

between the two ports in the microstrip line path as shown in Fig. 1(a). Also, to focus mainly on the performance of the active element, an ideal phase shifter is considered in the structure to control the phase of the reflected signal. Dielectric constant of top substrate is 3.02 with a height of 1.524 mm, and dielectric constant of bottom substrate is 6.15 with a height of 1.28 mm. The element is designed in the center frequency of 6 GHz by adjusting the dimensions of the patch, aperture, and matching stub so that good matching is achieved from the ports at the end of the microstrip lines and also increasing the isolation between the two slots. Optimized dimensions for the element are given in Table 1.

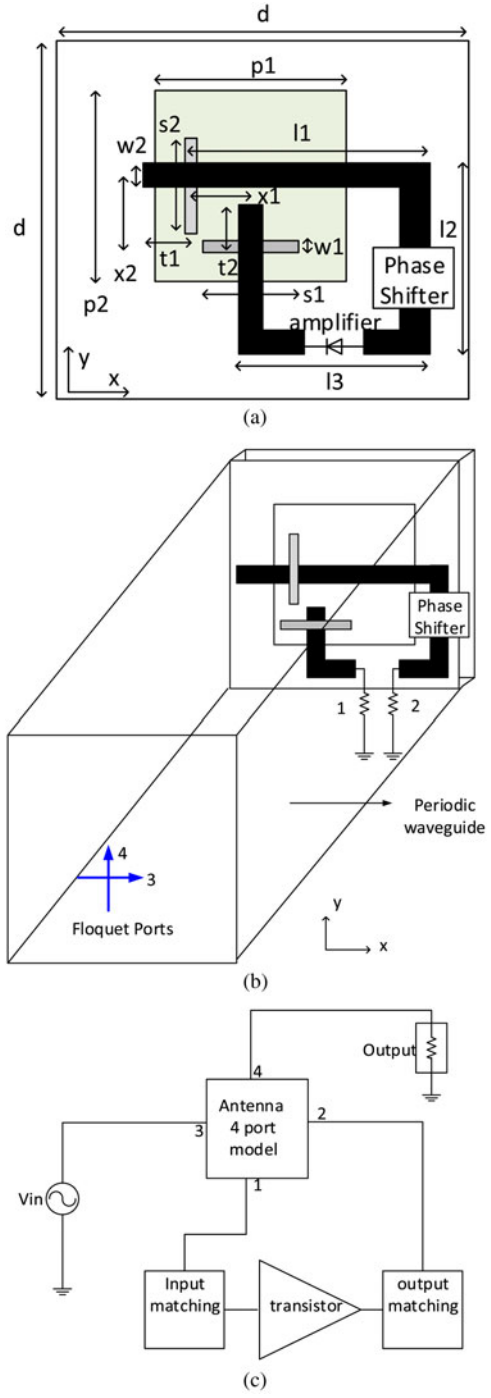

Fig. 1. (a) Antenna unit cell schematic, (b) four port modeling of the unit cell, and (c) nonlinear simulation of active element.

A) Unit cell modeling

To simulate the unit cell of the antenna assuming infinite array, the active element is replaced by a two port network and the unit cell is modeled as a four port network, in which ports 3 and 4 are spatial ports modeled as Floqute port, and ports 1 and 2 are located at the middle of the transmission lines representing the amplifier. Consequently, linear structure is simulated by high frequency structure simulator version 13 software to obtain four port scattering parameters as shown in Fig. 1(b). In this simulation, phase shifter is replaced by a transmission line and infinite array approach is used which gives a good approximation of the reflected phase from the element using Floquet modes [19].

B) Active unit cell modeling

After modeling the linear part of the unit cell, active element is added to the analysis by a nonlinear two port network as shown in Fig. 1(c).

Showing the analysis procedure needs to select a sample transistor in which its nonlinear model parameters are available. Also, as our goal is to compare analysis results with ADS simulation for verification, nonlinear model should be defined in the software. By the explained nonlinear analysis method, the analysis procedure can be performed for other transistors with different nonlinear models. Active element used in this section is ATF36163 which has nonlinear Statz model [20]. This model is shown in Appendix.

III. NONLINEAR ANALYSIS

A) Harmonic balance analysis

The model for analyzing the antenna is complex and the unit cell response of the amplifying reflectarray antenna should be obtained for all input powers of the amplifiers.

Nonlinear analysis is performed using harmonic balance method which is appropriate for nonlinear circuit analysis and is commonly used to simulate nonlinear circuits. Therefore, using harmonic balance method [21], nonlinear analysis of the unit cell is performed. For this reason, the unit cell structure is divided into two nonlinear and linear networks as shown in Fig. 2(a). The linear subcircuit is treated as a multiport and described by its Y-parameters and the nonlinear elements are modeled by their I/V or Q/V characteristics, given in (A.1)–(A.5) in the appendix, and must be analyzed in the time-domain. The nonlinear network is composed of two nonlinear capacitances and one nonlinear current source and the linear network consists of parasitic elements and lumped elements of unit cell and also, four-port network of the unit cell obtained in the previous section.

The circuit in Fig. 2(a) is successfully analyzed when either the steady-state voltage or current waveforms at each port are known [21]. If, for example, we know the frequency domain port voltages, we can use the Y-parameter matrix of the linear subcircuit to find the port currents. The port currents can also be found by inverse-Fourier transforming the voltages to obtain their time-domain waveforms and calculating the current waveforms from the nonlinear elements' I/V equations. Our aim in harmonic balance analysis is to find a set of port voltage waveforms that give the same currents in both the

https://doi.org/10.1017/S1759078715001750 Published online by Cambridge University Press

Table 1. Parameters of the cell.

Parameter	d	P1	P2	S1	S2	Wl
Value	33.56 mm	14.3 mm	13.9 mm	6.3 mm	8.8 mm	0.75 mm
Parameter	t1	t2	w2	x1	x2	l1
Value	6 mm	2.5 mm	1.87 mm	1.5 mm	5.7 mm	20.7 mm
Parameter	l2	l3				
Value	12 mm	14.8 mm				

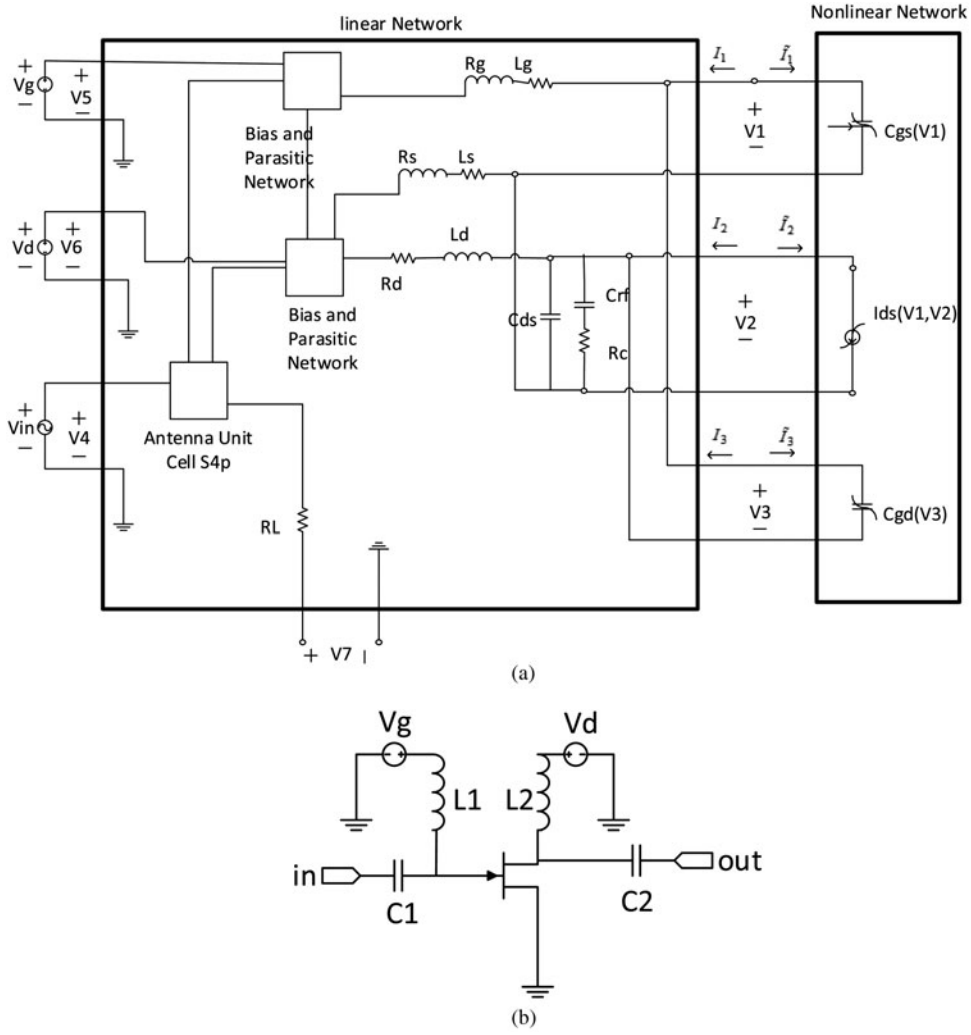

Fig. 2. (a) Dividing the unit cell to nonlinear and linear networks, (b) biasing network of the amplifier.

linear-network equations and the nonlinear-network equations; that is, the currents satisfy Kirchoff's current law. When that set is found, it must be a solution. Therefore, our aim is to find voltages of V_1, V_2, and V_3 of Fig. 2(a), to have $I_i + \tilde{I}_i = 0$ and $i = 1,2,3$. Biasing network of the amplifier is shown in Fig. 2(b), where DC bias voltages of gate and drain are -0.2 and 1.5 (V), respectively, and capacitances C1 and C2 are 100 (nF), and inductances L1 and L2 are 100 (nH). Detailed steps to obtain harmonic balance equation and solving it, is explained in the Appendix.

Considering nonlinear Statz model for the transistor and harmonic balance analysis, total directivity of the unit cell and the phase shift of the reflected signal from the cell are obtained versus incident power to the unit cell which are shown in Figs 3(a) and 3(b). Besides, to verify our code, nonlinear results of harmonic balance analysis is compared with ADS software simulation in Figs 3(a) and 3(b) which have good agreement. Nonlinear simulation can be performed using other simulation software too. Schematic of the nonlinear simulation and nonlinear analysis is shown in Fig. 1(c) where the nonlinear active element is placed between ports 1 and 2 in Fig. 1(b). Pin in Figs 3(a) and 3(b) is the power of port 3 of Fig. 1(c) which simulates the incident plane wave. Gain of the unit cell is obtained from the ratio of the power delivered to port 4; which indicates the reflected wave in the orthogonal polarization; to the input power of port 3 in Fig. 1(c).

https://doi.org/10.1017/S1759078715001750 Published online by Cambridge University Press

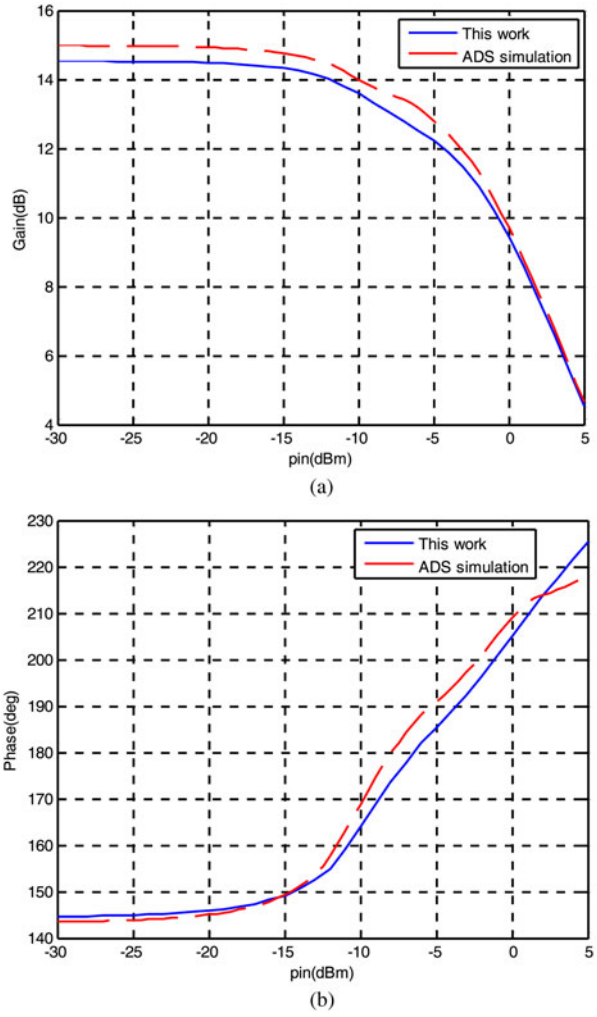

Fig. 3. (a) Gain response of the active unit cell by nonlinear analysis, (b) phase response of the active unit cell by nonlinear analysis.

B) Investigating distortion caused by active element

It is interesting to investigate the impact of nonlinearities on system level parameters of reflectarrays, such as harmonic distortion, especially given the spatially dispersive nature of the reflectarray with respect to out-of-band frequencies. This analysis can be performed if the nonlinear model of the active element is available and the explained method in the previous sections is used to obtain nonlinear behavior of the active reflectarray antenna. Therefore, in this section harmonic distortion is evaluated utilizing nonlinear model of the amplifier. Harmonic levels versus input power to the active unit cell is depicted in Fig. 4 which shows an increase in the harmonic levels as the input power to the cell increases, because nonlinearity increases. The analysis method to obtain harmonic distortion is like the analysis used to obtain the gain and the phase response of the active nonlinear unit cell. Second-harmonic level distortion indicates the ratio of the power of the second-harmonic component to the power of the fundamental frequency and the third-harmonic level distortion indicates the ratio of the power of the third-harmonic component to the power of the fundamental frequency which is shown in Fig. 4.

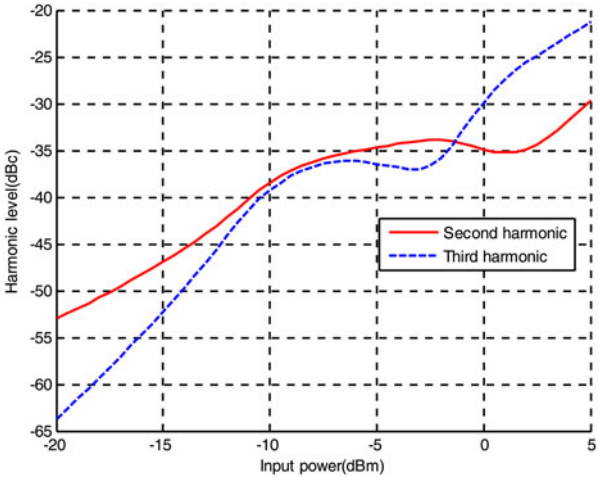

Fig. 4. Harmonic levels versus input power to the active unit cell.

IV. SAMPLE AMPLIFYING REFLECTARRAY DESIGN

In this section, we show that the power received to each cell is different and as a result each cell may have different gain and phase. To simulate the active antenna, a $59.5 \times 59.5\ \text{cm}^2$ antenna is designed by focal length of 74 cm. Assuming center of reflectarray as center of Cartesian coordinates, feed antenna is placed in (-29.6, 0, and 74 cm).

We should determine the compensating phase of each element to have a focused beam in the desired direction. Our antenna contains 17×17 reflecting elements that are illuminated by a feed located at the focal point of the antenna. Considering a horn feed illuminating the individual patches of the antenna, the excitation terms are proportional to the magnitude and phase of the electric field of the feed at the nth patch. One factor that affects the reflected field at each patch is the distance between the feed phase center and the nth element phase center (R_n). Furthermore, the feed has a certain angular taper over the antenna surface which can be included in the pattern analysis by multiplying the relative complex excitation term by a raised cosine factor [19] that can be adjusted to match the pattern of the actual feed by choosing the proper q. Here, q is the exponent of the feed pattern function represented by $\cos^q\theta$ and is determined from the taper factor at the edges of the reflectarray, which is about -10 dB for a focused beam [19]. The angular taper of the feed can be modeled as $e^{-jkR_n}/R_n \cos\theta_n^q$. Consequently, by multiplying the complex excitation term by the compensating phase and amplitude factor $A_n.e^{-jk\psi_n}$ resulted from each element, the complex reflected field from each element can be expressed in the form

$$A_n \frac{\cos\theta_n^q}{|R_n|} e^{-j(kR_n-\psi_n)}, \tag{1}$$

in which ψ_n is the compensation phase of the nth element.

The required phase shift at each element to produce a collimated beam in a given direction is [19]:

$$\phi_n = k_o(R_n - (x_n \cos\phi_b + y_n \sin\phi_b)\sin\theta_b), \tag{2}$$

where θ_b, ϕ_b shows the beam direction, k_o is the free space propagation constant, R_n is the distance between the feed

https://doi.org/10.1017/S1759078715001750 Published online by Cambridge University Press

phase center and the nth element phase center, and (x_n, y_n) are the coordinates of element n.

Considering the raised cosine factor $\cos^q\theta$ for the feed pattern function with $q = 13$, relative power imposed by the feed horn antenna on the reflectarray antenna surface is obtained which is shown in Fig. 5(a). Relative power on the antenna surface shows the power distribution on the reflectarray antenna surface relative to the maximum power on the antenna surface. Also, required phase shift of each cell of the antenna based on (A.18) is shown in Fig. 5(b).

A) Case 1

By varying the power of the feed antenna, the power distribution on the reflectarray antenna surface changes. Assuming transmitted feed antenna power in a way that the power distribution on the antenna surface is like Fig. 6(a), most active elements are nonlinear, and the impact of nonlinearity of each cell should be considered. For this reason, amplitude and phase differences caused by the nonlinear amplifier in each cell should be considered.

Considering amplitude and phase nonlinear behavior of the unit cell shown in Figs 3(a) and 3(b), and the power distribution on the antenna surface shown in Fig. 6(a), amplitude and phase error of each unit cell are calculated as shown in Figs 6(b) and 6(c). In this case, gain of the amplifiers is shown in Fig. 6(b) which varies from 4 to 13 dB, and the errors caused by the amplifiers in the phase of the reflected wave are shown in Fig. 6(c) which is 45°.

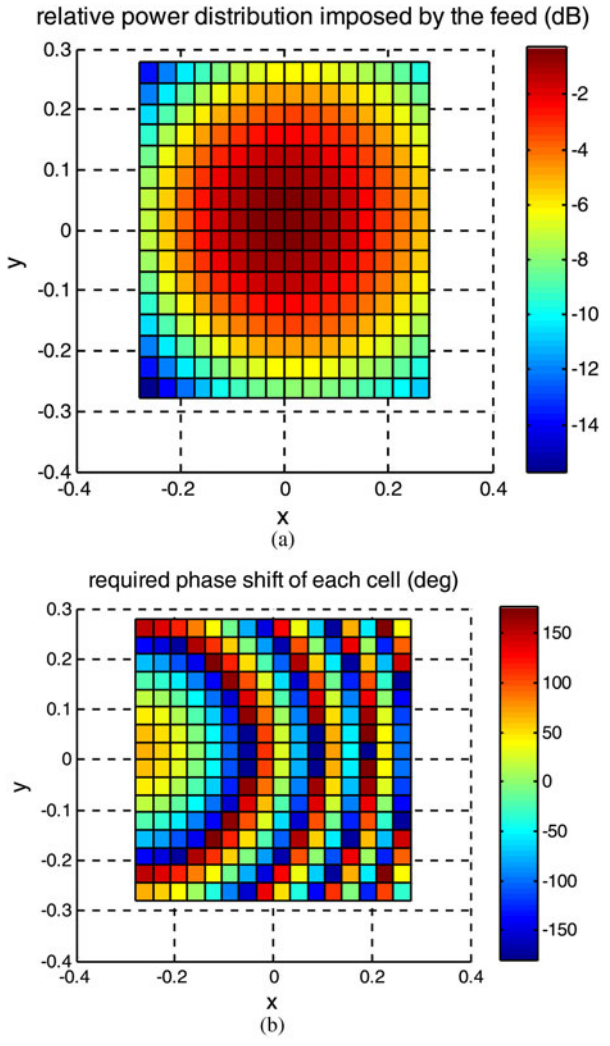

Fig. 5. (a) Relative power imposed by the feed horn antenna on the reflectarray antenna surface, (b) required phase shift of each cell of the antenna based on (A.18).

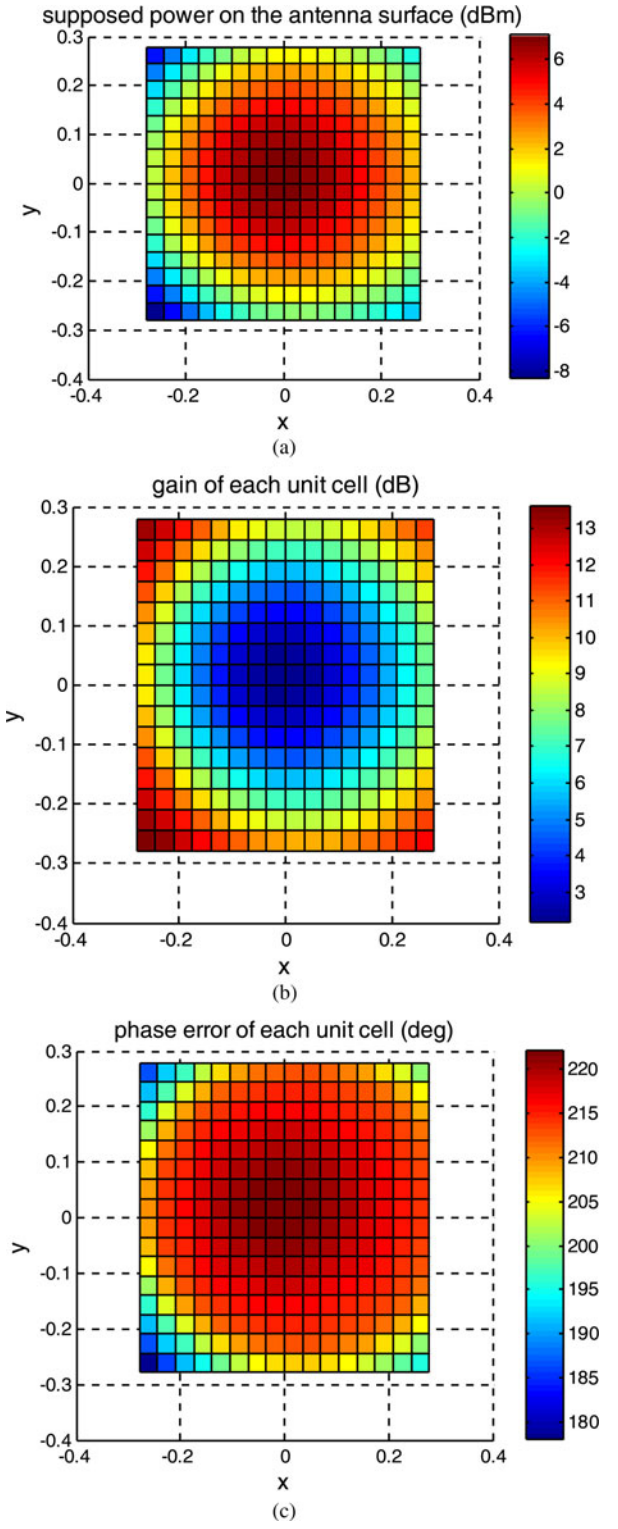

Fig. 6. Case 1: when feed power is so that active elements are in nonlinear state: (a) supposed power on the antenna surface, (b) gain of each unit cell, (c) phase error of each unit cell.

https://doi.org/10.1017/S1759078715001750 Published online by Cambridge University Press

B) Case 2

Assuming transmitted feed antenna power in a way that the power distribution on the antenna surface is like Fig. 7(a), most active elements are linear. In this case, gain of the amplifiers is shown in Fig. 7(b) which varies in an acceptable range from 14.3 to 14.9 dB. Also, the errors caused by the amplifiers in the phase of the reflected wave are shown in Fig. 7(c) which is 14°.

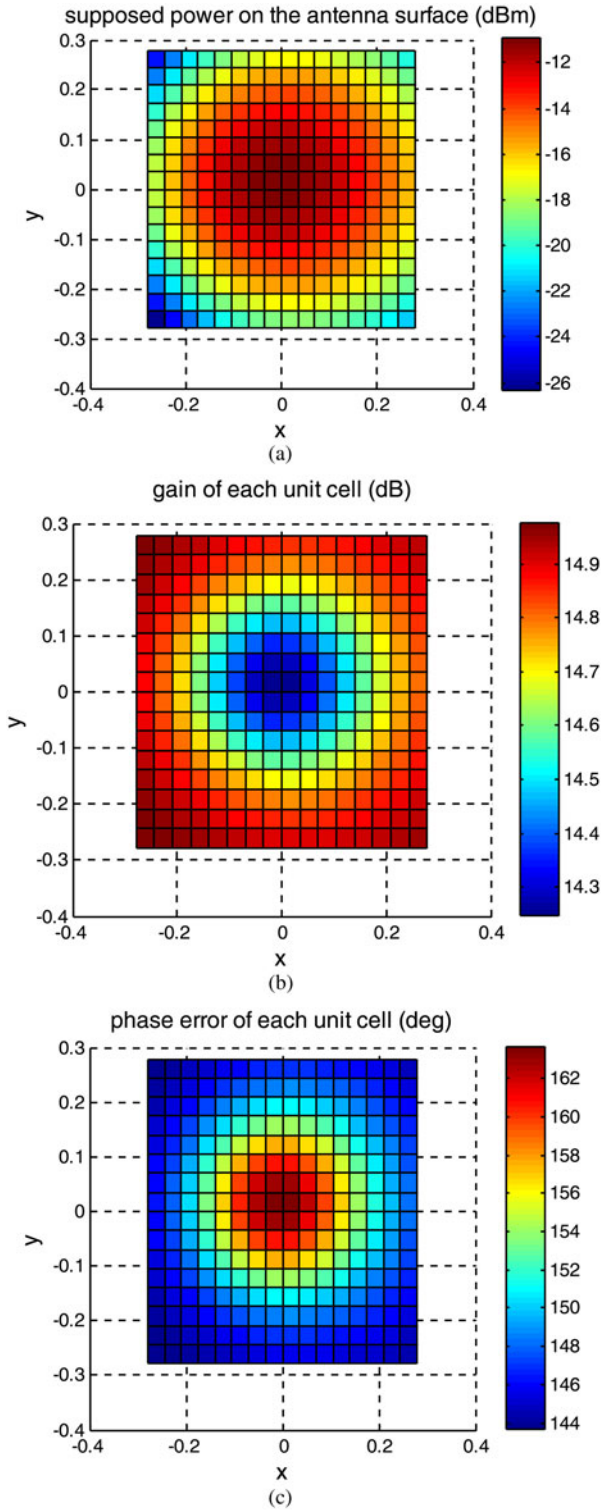

Fig. 7. Case 2: when feed power is so that active elements are in linear state: (a) supposed power on the antenna surface, (b) gain of each unit cell, (c) phase error of each unit cell.

C) Computing directivity for case 1 and case 2

Directivity of the antenna can be computed using the input power of the feed horn P_F, according to [19] as:

$$D(\theta, \varphi) = \frac{4\pi r^2}{2\eta_o P_F} |E(\theta, \varphi)|^2, \quad (3)$$

where η_o is the intrinsic impedance of the free space and $|E(\theta, \varphi)|$ is the amplitude of the far electric field. Hence, far electric field should be calculated to obtain directivity of the antenna which is explained in [19].

The errors in the amplitude and phase of the reflected signal from each cell can cause gain reduction. Antenna directivity with and without considering the nonlinear effect of active elements are shown in Fig. 8(a) for case 1 and Fig. 8(b) for case 2. In Fig. 8(a) feed power is like Fig. 6(a) so that some cells are in nonlinear region. In this case, nonlinear analysis shows degradation in gain which cannot be assessed by linear analysis. In another scenario, in Fig. 8(b) feed power is like Fig. 7(a) so that all cells are in linear

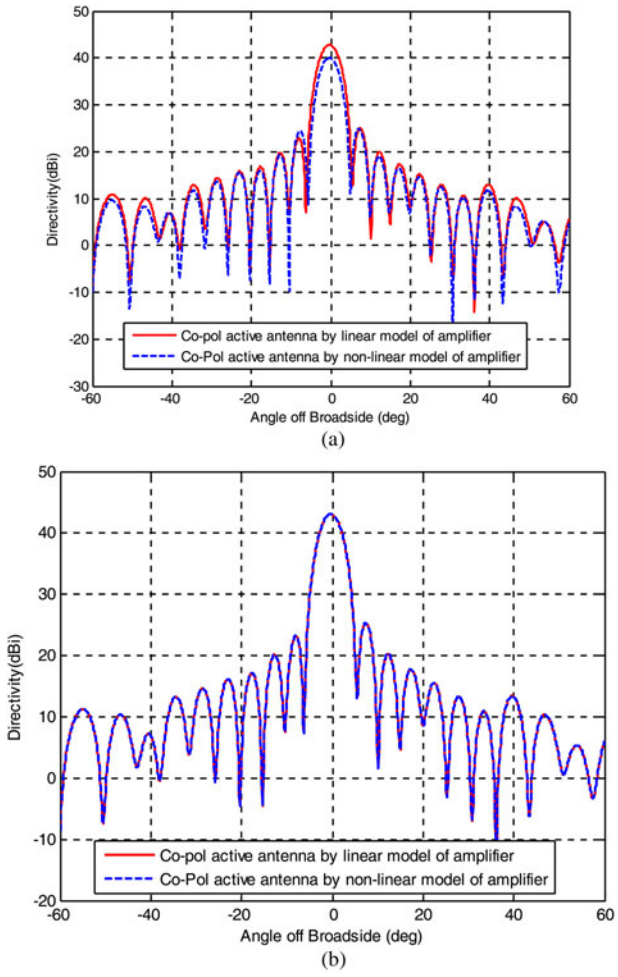

Fig. 8. (a) Antenna directivity with and without considering the nonlinear effect of active elements when feed power is so that some cells are in nonlinear region, (b) antenna directivity with and without considering the nonlinear effect of active elements when feed power is so that all cells are in linear region.

https://doi.org/10.1017/S1759078715001750 Published online by Cambridge University Press

Table 2. Lost gain versus amount of nonlinearity.

K (dB)	0	0.7	1.2	1.6	2.2	3	4.5	6	8	9	10
Lost gain (dB)	0	0.1	0.19	0.35	0.49	0.63	0.85	1.17	1.67	2.34	3.4

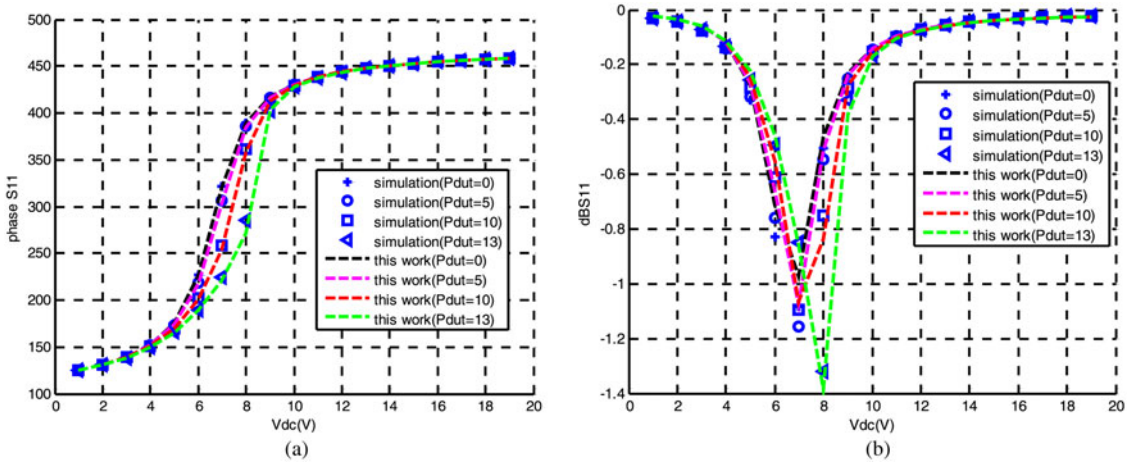

Fig. 9. (a) Phase response of the active unit cell by nonlinear analysis, (b) amplitude response of the active unit cell by nonlinear analysis.

region where linear and nonlinear simulations have the same result. Therefore, to assess the pattern of the active reflectarray antenna correctly, for all feed power, the nonlinear impact of amplifier should be considered.

To relate the amount of directivity lost to the area of nonlinearity of the amplifiers, first the amount of nonlinearity of the amplifiers should be defined which is proposed by the maximum gain of the amplifiers of the array minus minimum gain of the amplifiers of the array for a supposed feed power as:

$$K = Gain_{max} - Gain_{min}. \quad (4)$$

Increase in K means that the array is more nonlinear. Now, lost gains for different K values are computed as in Table 2.

V. VERIFICATION OF THE PROPOSED NONLINEAR ANALYSIS

We have repeated the analysis method described in this paper for the unit cell of [9] to verify our analysis method by test results of [9]. Test results of [9] show nonlinear behavior of the active reflectarray cell but [9] does not give analysis or simulation results for this nonlinear behavior.

In [9] required phase shift of each cell is obtained by changing DC voltage of the two varactor diodes and the amplitude of the reflected wave from the surface of the reflectarray is imposed by the feed antenna. Like the described method in Section II and III, the active elements are replaced by two port networks and the unit cell is modeled as a six port network. Consequently, linear structure is simulated by HFSS software to obtain six port scattering parameters assuming infinite array. After modeling the linear part of the unit cell, active elements are added to the analysis by two nonlinear two port networks and phase response and amplitude response of the active unit cell is obtained for different incident power levels of the feed antenna by both nonlinear analysis, and nonlinear simulation using ADS software, which is shown in Fig. 9. Test results shown in Fig. 4 of [9] is near the results of Fig. 9. So, our nonlinear analysis procedure is verified by test results. However, because the parameters of the diode model are not specified in [9], the selected parameters for the varactor diode in this paper are different, and this leads to different cell response. Nonlinear diode model is given in [18] and diode parameters used in this paper are given in Table A.2 of Appendix C.

VI. CONCLUSION

The importance of considering nonlinear behavior of amplifying reflectarray is clarified and it is shown that in some cases, nonlinear analysis of amplifying reflectarray antenna is necessary. Thus, nonlinear analysis of active reflectarray antenna has been explained using harmonic balance method in which scattering parameters of the passive part of the unit cell is obtained and used in the nonlinear analysis to obtain nonlinear response of the unit cell and harmonic distortion versus incident power. Analysis result is verified by comparing with simulation using advanced design system (ADS) software. Finally, the result of nonlinear analysis has been used in designing a sample antenna which shows error in predicting pattern of the antenna with linear modeling of the active element.

ACKNOWLEDGEMENTS

The authors thank Mr. Hamed Golestaneh for his helpful comments.

REFERENCES

[1] Pozar, D.; Metzler, T.: Analysis of a reflectarray antenna using microstrip patches of variable size. Electron. Lett., **29** (1993), 657–658.

[2] Hasani, H.; Kamyab, M.; Mirkamali, A.: Low cross-polarization reflectarray antenna. IEEE Trans. Antennas Propag., **59** (2011), 1752–1756.

https://doi.org/10.1017/S1759078715001750 Published online by Cambridge University Press

[3] Malfajani, R.S.; Atlasbaf, Z.: Design and implementation of a broadband single-layer reflectarray antenna with large-range linear phase elements, IEEE Antennas Wireless Propag. Lett., **11** (2012), 1442–1445.

[4] Bialkowski, M.; Song, H.: Dual linearly polarized reflectarray using aperture coupled microstrip patches, Antennas and Propagation Society Int. Symp., Boston, MA, USA, 2001.

[5] Venneri, F.; Costanzo, S.; Massa, G.Di.; Amendola, G.: Aperture-coupled reflectarrays with enhanced bandwidth features. J. Electromagn. Waves Appl., **22** (2008), 1527–1537.

[6] Makdissy, T.; Gillard, R.; Fourn, E.; Girard, E.; Legay, H.: Phase-shifting cell for dual linearly polarized reflectarrays with reconfigurable potentialities. IEEE Antennas Wireless Propag., **13**, (2013), 11–14.

[7] Venneri, F.; Costanzo, S.; Massa, G.Di.: Design and validation of a reconfigurable single varactor-tuned reflectarray. IEEE Trans. Antennas Propag., **61** (2013), 635–645.

[8] Bayraktar, O.; Civi, O.A.; Akin, T.: Beam switching reflectarray monolithically integrated with RF MEMS switches. IEEE Trans. Antennas Propag., **60** (2012), 854–862.

[9] Riel, M.; Laurin, J.: Design of an electronically beam scanning reflectarray using aperture-coupled elements IEEE Trans. Antennas Propag., **55** (2007), 1260–1266.

[10] Venneri, F.; Costanzo, S.; Massa, G.Di.: Reconfigurable aperture-coupled reflectarray element tuned by single varactor diode. Electron. Lett., **48** (2012), 68–69.

[11] Georgiadis, A.; Collado, A.: Nonlinear analysis of a reflectarray cell based on a voltage-controlled oscillator, Antennas and Propagation Society Int. Symp., San Diego, CA, 2008.

[12] Georgiadis, A.; Collado, A.: Active reconfigurable reflectarray based on voltage-controlled oscillators, IEEE Int. Symp. Phased Array Systems and Technology (ARRAY), Waltham, MA, 2010.

[13] Nguyen, B.D.; Pham, K.T.; Tran, V.-S.; Mai, L.; Yonemoto, N.; Kohmura, A. et al.: Electronically tunable reflectarray element based on C-patch coupled to delay line. Electron. Lett., **50** (2014), 1114–1116.

[14] Perez-Palomino, G.; Florencio, R.; Encinar, J.A.; Barba, M.; Dickie, R.; Cahill, R. et al.: Accurate and efficient modeling to calculate the voltage dependence of liquid crystal based reflectarray cells. IEEE Trans. Antennas Propag., **62** (2014), 2659–2668.

[15] Kishor, K.K.; Hum, S.V.: An amplifying reconfigurable reflectarray antenna. IEEE Trans. Antennas Propag., **60** (2012), 197–205.

[16] Bialkowski, M.E.; Robinson, A.W.; Song, H.J.: Design, development, and testing of X-band amplifying reflectarrays. IEEE Trans. Antennas Propag., **50** (2002), 1065–1076.

[17] Clark, R.W.; Huff, G.H.; Bernhard, J.T.: An integrated active microstrip reflectarray element with an internal amplifier IEEE Trans. Antennas Propag., **51** (2003), 993–999.

[18] Antognetti, P.; Massobrio, G.; Massobrio, G.: Semiconductor Device Modeling with SPICE, McGraw-Hill, New York, 1993.

[19] Huang, J.: Reflectarray Antenna, Wiley Online Library, Hoboken, New Jersey, 2008.

[20] Statz, H.; Newman, P.; Smith, I.W.; Pucel, R.A.; Haus, H.: GaAs FET device and circuit simulation in SPICE. IEEE Trans. Electron. Devices, **34** (1987), 160–169.

[21] Maas, S.A.: Nonlinear Microwave and RF Circuits, Artech House, Norwood, MA, 2003.

[22] Golestaneh, H.; Abdipour, A.; Mohammadi, A.: Nonlinear modeling and analysis of a Doherty power amplifier driven by non-constant envelope signals. Analog Integr. Circuits Signal Process., **72** (2012), 141–153.

APPENDIX

A. STATZ MODEL

Statz model which has two nonlinear capacitances of C_{gs} and C_{gd}, and one nonlinear current source of I_{ds} is shown in Fig. 10.

Relations for current source of I_{ds}, electric charges of Q_{gs} and Q_{gd}, and capacitances of C_{gs} and C_{gs} in Statz model are given in (A.1)–(A.5) and parameters of the nonlinear model of ATF36163 are given in Table A.1. Current source of I_{ds} in Statz model is given as [20]:

$$I_{ds}=\begin{cases}\dfrac{\beta\left(V_{gs}-Vt_o\right)^2}{1+b\left(V_{gs}-Vt_o\right)}\left[1-\left[1-\dfrac{\alpha V_{ds}}{3}\right]^3\right](1+\lambda V_{ds}) & 0<V_{ds}<3/\alpha \\ \dfrac{\beta\left(V_{gs}-Vt_o\right)^2}{1+b\left(V_{gs}-Vt_o\right)}(1+\lambda V_{ds}) & V_{ds}\geq 3/\alpha\end{cases} \tag{A.1}$$

Also, electric charges of Q_{gs} and Q_{gd} are expressed as:

$$Q_{gs}=\begin{cases}C_{gso}\left[2\times V_{bi}\left(1-\sqrt{1-\dfrac{V_{max}}{V_{bi}}}\right)+\dfrac{V_{new}-V_{max}}{\sqrt{1-V_{max}/V_{bi}}}\right] & V_{new}>V_{max} \\ C_{gso}\times 2\times V_{bi}\left(1-\sqrt{1-\dfrac{V_{new}}{V_{bi}}}\right) & V_{new}\leq V_{max}\end{cases} \tag{A.2}$$

$$Q_{gd}=C_{gdo}\times V_{eff2}. \tag{A.3}$$

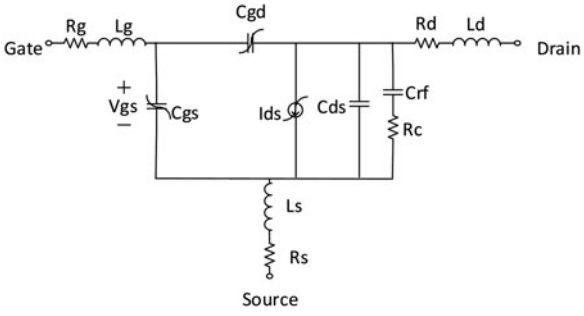

Fig. 10. Nonlinear Statz model of the transistor.

Table A1. Statz model Parameters of ATF36163.

Parameter	Value	Units	Parameter	Value	Units
V_{t_o}	−0.55	V	R_s	0.5	Ohm
β	0.1	A/V²	L_d	0.04e-9	H
λ	0.25	1/V	L_g	0.03e-9	H
α	5	1/V	L_s	0.01e-9	H
b	1.5	_	C_{ds}	0.05e-12	F
V_{bi}	0.7	V	C_{rf}	0.1	F
C_{gso}	0.13e-12	F	R_c	350	Ohm
C_{gdo}	0.04e-12	F	Delta1	0.2	V
R_d	0.5	Ohm	Delta2	0.2	V
R_g	1	Ohm			

https://doi.org/10.1017/S1759078715001750 Published online by Cambridge University Press

Moreover, capacitances of C_{gs} and C_{gd} in Statz model are obtained as:

$$C_{gs}=\frac{\partial Q_{gs}}{\partial V_{gs}}+\frac{\partial Q_{gd}}{\partial V_{gs}}=$$

$$\begin{cases}\dfrac{C_{gso}}{2\sqrt{1-V_{max}/V_{bi}}}\left[1+\dfrac{V_{eff1}-V_{t_o}}{\sqrt{\left(V_{eff1}-V_{t_o}\right)^2+Delta2^2}}\right]\times \\ \dfrac{1}{2}\times\left(1+\dfrac{V_{gs}-V_{gd}}{\sqrt{\left(V_{gs}-V_{gd}\right)^2+Delta1^2}}\right)+V_{new}>V_{max} \\ \dfrac{C_{gdo}}{2}\left(1-\dfrac{V_{gs}-V_{gd}}{\sqrt{\left(V_{gs}-V_{gd}\right)^2+Delta1^2}}\right), \\ \dfrac{C_{gso}}{2\sqrt{1-V_{new}/V_{bi}}}\left[1+\dfrac{V_{eff1}-V_{t_o}}{\sqrt{\left(V_{eff1}-V_{t_o}\right)^2+Delta1^2}}\right]\times \\ \dfrac{1}{2}\times\left(1+\dfrac{V_{gs}-V_{gd}}{\sqrt{\left(V_{gs}-V_{gd}\right)^2+Delta2^2}}\right)+V_{new}\le V_{max} \\ \dfrac{C_{gdo}}{2}\left(1-\dfrac{V_{gs}-V_{gd}}{\sqrt{\left(V_{gs}-V_{gd}\right)^2+Delta2^2}}\right)\end{cases} \tag{A.4}$$

$$C_{gd}=\frac{\partial Q_{gd}}{\partial V_{gd}}+\frac{\partial Q_{gs}}{\partial V_{gd}}=$$

$$\begin{cases}\dfrac{C_{gso}}{2\sqrt{1-V_{max}/V_{bi}}}\left[1+\dfrac{V_{eff1}-V_{t_o}}{\sqrt{\left(V_{eff1}-V_{t_o}\right)^2+Delta1^2}}\right]\times \\ \dfrac{1}{2}\times\left(1-\dfrac{V_{gs}-V_{gd}}{\sqrt{\left(V_{gs}-V_{gd}\right)^2+Delta2^2}}\right)+V_{new}>V_{max} \\ \dfrac{C_{gdo}}{2}\left(1+\dfrac{V_{gs}-V_{gd}}{\sqrt{\left(V_{gs}-V_{gd}\right)^2+Delta2^2}}\right), \\ \dfrac{C_{gso}}{2\sqrt{1-V_{new}/V_{bi}}}\left[1+\dfrac{V_{eff1}-V_{t_o}}{\sqrt{\left(V_{eff1}-V_{t_o}\right)^2+Delta1^2}}\right]\times \\ \dfrac{1}{2}\times\left(1+\dfrac{V_{gs}-V_{gd}}{\sqrt{\left(V_{gs}-V_{gd}\right)^2+Delta2^2}}\right)+V_{new}\le V_{max} \\ \dfrac{C_{gdo}}{2}\left(1-\dfrac{V_{gs}-V_{gd}}{\sqrt{\left(V_{gs}-V_{gd}\right)^2+Delta2^2}}\right)\end{cases} \tag{A.5}$$

where Delta1 and Delta2 are two parameters of the nonlinear model. Delta1 is the capacitance saturation transition voltage and Delta2 is the capacitance threshold transition voltage which are given in Table A.1. Furthermore, V_{new}, V_{eff1}, and V_{eff2} are defined as:

$$V_{new}=\frac{1}{2}\left(V_{eff1}+V_{t_o}\right)+\sqrt{\left(V_{eff1}-V_{t_o}\right)^2+Delta2^2}, \tag{A.6}$$

$$V_{eff1}=\frac{1}{2}\left[\left(V_{gs}+V_{gd}\right)+\sqrt{\left(V_{gs}-V_{gd}\right)^2+Delta1^2}\right], \tag{A.7}$$

$$V_{eff2}=\frac{1}{2}\left[\left(V_{gs}+V_{gd}\right)-\sqrt{\left(V_{gs}-V_{gd}\right)^2+Delta1^2}\right]. \tag{A.8}$$

B. DETAILS OF HARMONIC BALANCE ANALYSIS

1) Currents of the linear part

Current of the linear sub circuit can be expressed as:

$$\begin{bmatrix}I_1\\I_2\\\vdots\\I_7\end{bmatrix}=\begin{bmatrix}Y_{11}&Y_{12}&\dots&Y_{17}\\Y_{21}&Y_{22}&\dots&Y_{27}\\\vdots&\vdots&\vdots&\vdots\\Y_{71}&Y_{72}&\cdots&Y_{77}\end{bmatrix}\begin{bmatrix}V_1\\V_2\\\vdots\\V_7\end{bmatrix}. \tag{A.9}$$

Partitioning the Y matrix in (A.9) gives an expression for I, the vector of currents of linear part in ports 1–3:

$$I=\begin{bmatrix}I_1\\I_2\\I_3\end{bmatrix}=\begin{bmatrix}Y_{11}&Y_{12}&Y_{13}\\Y_{21}&Y_{22}&Y_{23}\\Y_{31}&Y_{32}&Y_{33}\end{bmatrix}\begin{bmatrix}V_1\\V_2\\V_3\end{bmatrix}$$
$$+\begin{bmatrix}Y_{14}&Y_{15}&Y_{16}&Y_{17}\\Y_{24}&Y_{25}&Y_{26}&Y_{27}\\Y_{34}&Y_{35}&Y_{36}&Y_{37}\end{bmatrix}\begin{bmatrix}V_4\\V_5\\V_6\\V_7\end{bmatrix}=Y_L.V+Y_S.V_S. \tag{A.10}$$

$I_S=Y_S.V_S$ represents a set of current sources in parallel with the first, second, and third ports; which transforms the input and output port excitations into this set of current sources.

2) Currents of the nonlinear part

Fourier transforming the charge waveform at each port gives the charge vectors for the capacitors at each port:

$$F\{q_{gs}(t)\}\rightarrow Q_{gs},\ F\{q_{gd}(t)\}\rightarrow Q_{gd}, \tag{A.11}$$

https://doi.org/10.1017/S1759078715001750 Published online by Cambridge University Press

and the charge vector, Q, is:

$$Q = \begin{bmatrix} Q_{gs} \\ o \\ Q_{gd} \end{bmatrix}. \tag{A.12}$$

The nonlinear-capacitor current is the time derivative of the charge waveform. Taking the time derivative corresponds to multiplying by $j\omega$ in the frequency domain, so:

$$\begin{aligned} & i_c(t) = \frac{dq(t)}{dt} \leftrightarrow jk\omega_P Q \qquad k = 0, 1, \ldots, K, \\ & \Rightarrow I_c = j\Omega Q \end{aligned} \tag{A.13}$$

where Ω is a diagonal matrix with three cycles of 0, ω_o, …, $k\omega_o$ along the main diagonal where $k = 0, 1, 2, \ldots$ is the number of harmonics determined.

Fourier transforming from nonlinear current vector in time-domain gives the nonlinear current vector in frequency domain:

$$F(i_{ds}(t)) \rightarrow I_{ds}. \tag{A.14}$$

Therefore, vector of nonlinear current sources in ports 1, 2, and 3, I_G is:

$$I_G = \begin{bmatrix} o \\ I_{ds} \\ o \end{bmatrix}. \tag{A.15}$$

So, nonlinear current vector of ports 1, 2, and 3 is $\tilde{I} = I_G + I_C$.

3) Solving harmonic balance equation

By calculating the admittance parameters of the linear network of Fig. 2(a), which is a 7×7 matrix, the following harmonic balance equation is obtained by substituting I and $\tilde{I}$ in $I_i + \tilde{I}_i = 0$ [21]:

$$F(v) = Y_L.V + I_s + j\Omega Q + I_G = 0, \tag{A.16}$$

where $y_{m,n} = diag(y_{m,n}(k\omega_c))$, and V is the vector of nonlinear voltages of the nonlinear ports.

The time-domain voltage waveforms at each port is obtained by inverse Fourier transform of the voltages at each port which is done in written matlab code by Ifft_Func command. Obtained time-domain voltages are used to calculate nonlinear current of (A.1) and nonlinear charges and capacitances of (A.2)–(A.5) which are in time-domain. The nonlinear-element currents result from two nonlinear capacitors, and one controlled source. Fourier transforming the charge and capacitance waveforms at each port gives the charge and capacitance vectors in frequency domain at each port which is done in written matlab code by fft command. Also, I_s current matrix is obtained from Y_s admittance matrix of (A.10). Obtained frequency domain currents and charges are used to obtain the harmonic balance equation of (A.16).

Harmonic balance equation can be solved with different methods, among which the Newton–Raphson [21] technique is the most common technique and is used in this paper. Newton–Raphson technique is an iterative method involving calculation of Jacobian matrix, which contains derivatives of all components of the vector $F(v)$, with respect to components of V and is expressed as [22]:

$$\begin{aligned} J_F &= \frac{\partial F_{(V)}}{\partial V} = Y_L + \frac{\partial I_{NL}}{\partial V} + j\Omega \frac{\partial Q_{NL}}{\partial V} \\ &= Y_L + J_I + j\Omega J_Q, \end{aligned} \tag{A.17}$$

$$\frac{\partial F_{n,k}}{\partial V_{m,l}} = Y_{n,m}(k = l) + \frac{\partial I_{NL\ n,k}}{\partial V_{m,l}} + jk\omega_c \frac{\partial Q_{NL\ n,k}}{\partial V_{m,l}}, \tag{A.18}$$

where n and m are the port indices (1, …, N), and k and l are the harmonic indices (0, …, H); hence, J_F will be a $N(H+1)$ by $N(H+1)$ matrix. Referring to (A.17) and (A.18) J_I and J_Q are written as:

$$J_I = \begin{bmatrix} o & o & o \\ G_m & G_{ds} & o \\ o & o & o \end{bmatrix}, \tag{A.19}$$

$$J_Q = \begin{bmatrix} C_{gs} & o & o \\ o & o & o \\ o & o & C_{gd} \end{bmatrix}. \tag{A.20}$$

G_m, G_{ds}, C_{gs}, and C_{gd} are $(H+1)$ by $(H+1)$ square matrices, expressed as:

$$A = \begin{bmatrix} A(0) & A(1) & \ldots & A(H-1) & A(H) \\ A^*(1) & A(0) & A(1) & \ldots & A(H-1) \\ \vdots & \vdots & \vdots & \ddots & \vdots \\ A^*(H) & A*(H-1) & \ldots & A^*(1) & A(0) \end{bmatrix}, \tag{A.21}$$

or, $A = toeplitz(A(1{:}H+1),\ conj(A(1{:}H+1)))$ in MATLAB notation. Note that in (A.21), $A(k)$ represents the kth frequency component of G_m, G_{ds}, C_{gs}, and C_{gd}, calculated in frequency-domain by taking fast fourier transform (FFT) of the time-domain values, G_m, G_{ds}, C_{gs}, and C_{gd}, respectively. G_m and G_{ds} denote derivatives of I_{ds} with respect to V_{gs} and V_{ds}, respectively.

C) DIODE PARAMETERS

Table A2. Diode parameters.

Symbol	Quantity	Value
I_s	Saturation current	100 (pA)
N	Ideal factor	2
V_t	Thermal voltage	26 (mV)
C_{jo}	Junction capacitance	1.7 (pF)
M	Grading coefficient	0.9
v_j	Junction potential	1.2
F_c	Forward-bias depletion capacitance coefficient	0.5
L_P	Parasitic inductance	0.4 (nH)
C_P	Parasitic capacitance	0.1 (pF)
R_s	Ohmic resistance	0.9 (Ohm)

https://doi.org/10.1017/S1759078715001750 Published online by Cambridge University Press

Iman Aryanian was born in Iran in 1986. He obtained his B.Sc. in Electrical Engineering and M.Sc. from Amirkabir University of Technology, Tehran, Iran in 2008 and 2010, respectively. He is presently working toward his Ph.D. program. His research interests are in the areas of reflectarray antenna, computational electromagnetic, semiconductor RF modeling, electromagnetic theory, and computational electromagnetics.

Abdolali Abdipour was born in Alashtar, Iran, in 1966. He received his B.Sc. degree in Electrical Engineering from Tehran University, Tehran, Iran, in 1989, his M.Sc. degree in Electronics from Limoges University, Limoges, France, in 1992, and his Ph.D. degree in Electronic Engineering from Paris XI University, Paris, France, in 1996. He is presently a professor with the Electrical Engineering Department, Amirkabir University of Technology (Tehran Polytechnic), Tehran, Iran. He has authored five books and has authored or coauthored over 290 papers in refereed journals and local and international conferences. His research areas include wireless communication systems (RF technology and transceivers), RF/microwave/millimeter-wave/THz circuit and system design, electromagnetic (EM) modeling of active devices and circuits, high-frequency electronics (signal-and-noise), nonlinear modeling, and analysis of microwave devices and circuits.

Gholamreza Moradi was born in Shahriar, Iran in 1966. He received his B.Sc. in Electrical Communication Engineering from Tehran University, Tehran, Iran in 1989, and his M.Sc. in the same field from Iran University of Science and Technology in 1993. Then he received his Ph.D. degree in Electrical Engineering from Tehran Polytechnic University, Tehran, Iran in 2002. His research areas include applied and numerical electromagnetics, microwave measurement and antenna. He has published more than 50 journal papers and has authored/coauthored five books in his major. He is presently an associate professor with the Electrical Engineering Department, Amirkabir University of Technology (Tehran Polytechnic), Tehran, Iran.

https://doi.org/10.1017/S1759078715001750 Published online by Cambridge University Press